32nd European Modeling & Simulation Symposium
17th International Multidisciplinary Modeling & Simulation Multiconference

ISSN 2724-0029 ISBN 978-88-85741-44-7 © 2020 The Authors.
DOI: 10.46354/i3m.2020.emss.049

Microstructured fibers with high birefringence and a wide spectral range of single-mode guidance

Alexander N. Denisov* and Sergei L. Semjonov

Prokhorov General Physics Institute of the Russian Academy of Sciences, Dianov Fiber Optics Research Center, 38 Vavilov Street, Moscow, 119333, Russia

*Corresponding author. Email address: denisov@fo.gpi.ru

Abstract

In this study the results of the numerical analysis of a new design of birefringent microstructured fibers (BMSFs) containing three rings of identical air holes around an elliptical core with different distances between the rings of holes are presented. The first ring contains two pairs of holes, which are more widely spaced than others. The BMSFs were characterized using the finite element method. Confinement losses for fundamental and higher-order modes were calculated in the spectral range of 0.20 to 2.65 microns. Simulation results show that an optimum configuration of the proposed design existed, for which the widest spectral range of single-mode guidance of fibers was obtained: from 0.2 to 2.3 microns.

Keywords: Microstructured fiber; photonic crystal fiber; single-mode fiber; birefringence; finite element method.

1. Introduction

Microstructured fibers (MSFs), also known as photonic crystal fibers (PCFs), with cores several micrometers in diameter and claddings with relatively large holes allow strong light confinement in their cores due to the high core-cladding refractive index contrast. As a result, such MSFs exhibit high non-linearity. Birefringent MSFs (BMSFs) are used in numerous applications in which light must be maintained in a linearly polarized state, and polarized supercontinuum generation presents specific interest for use in physical measurements and many scientific applications (Klarskov et al., 2011; Nielsen et al., 2007; Xiong and Wadsworth, 2008).

Numerous tasks also require high light-beam quality, which can be provided by single-mode fibers. MSFs with hexagonal structures of holes can be single-mode for any wavelength (so-called 'endlessly single-mode' fibers) (Birks et al., 1997). However, for these MSFs, a necessary condition exists for its structure, namely, $d/\Lambda < 0.406$ (Mortensen et al., 2003), where d is the diameter of holes and Λ is the distance between their centers. Simultaneously, the number of rings of holes must be sufficiently large (number of holes > 100) to ensure low propagation loss of the fundamental mode.

The purpose of this study is numerical investigation of a new design of birefringent microstructured fibers with relatively small number of holes (30). Confinement losses for fundamental mode and higher-order modes were calculated for different BMSF's configuration parameters. An optimum configuration of the proposed design was found, for which the widest spectral range of single-mode guidance was obtained: from 0.2 to 2.3 microns.

2. State of the art

To allow single-mode guidance of MSFs with a small

number of holes several fiber structures have been proposed in literature (Dong et al., 2007; Fini, 2005; Saini et al., 2016; Saitoh et al., 2011; Tsuchida et al., 2007; Wong et al., 2005). These MSFs are leakage channel fibers (LCFs) and they have one or two rings of large air holes. By precisely engineering the air-hole pitch Λ and diameter d, it is possible to selectively achieve a low propagation loss of the fundamental mode (FM) and at the same time increasing the losses for the higher-order modes (HOMs). However, single-mode guidance for these fibers may be achieved only for narrow spectral range.

In the paper (Fini, 2005) hole-assisted fibers have been proposed. The author (Fini, 2005) considered fiber geometry with doped core and two rings (with 6 holes for the first ring and 12 holes for the second ring) of identical circular air holes with hole spacing Λ_1 and Λ_2 for the first and the second rings of holes, respectively. Suppression of HOMs was explained as the result of index-matched coupling between these core and very leaky cladding modes. According to the author (Fini, 2005), for the proposed fiber geometry the fundamental mode, in principle, has zero confinement loss.

In the paper (Tsuchida et al., 2007) large-mode area (LMA) single mode MSFs have been proposed. Authors (Tsuchida et al., 2007) considered pure silica hexagonal fiber geometry with two rings (12 and 24 holes) of different circular air holes (with diameters d_1 and d_2 for the first ring, and d for the second ring) with the same hole's spacing Λ for both rings of holes. The air-hole diameters of d_1 and d_2 in the innermost air-hole ring can be tuned to enhance the confinement losses of the HOM. Additional enhancement of the confinement losses of the higher-order central-core mode can be achieved through the index-matching mechanism between the central-core and the ring-core modes. At the desired wavelength (λ = 1.064 μm) the confinement losses of the HOM have been enhanced up to a level of 1.4 dB/m. But the spectral range of the single-mode guidance of the proposed MSFs was about 0.1 microns.

We have earlier performed numerical and experimental investigations of the BMSF design with an elliptical core that is surrounded by two concentric rings of identical circular air holes (Denisov et al., 2015). The distance between the adjacent holes in the first ring is Λ except for one or two pairs of holes, which are a greater distance apart. Each of the holes of the second ring is at the same distance Λ from the two nearest holes of the first ring. We have selected ratio d/Λ = 0.95 to ensure a sufficiently low confinement losses of the fundamental mode. But estimation of the V parameter for this BMSF (with expression (4) from (Mortensen et al., 2003)) gives us the cutoff wavelength of about 6 microns. Consequently, this BMSF have many HOMs that have low leakage losses in a 1.55 microns' wavelength region.

In this study, we propose a new design of BMSF containing three rings of identical air holes around an elliptical core with different distances between the rings of holes. The distance between the adjacent holes in the first ring is constant except for two pairs of holes, which are a greater distance apart (i.e., they have two wider bridges). We demonstrate that the proposed design of the BMSF, at a certain relationship between the configuration parameters, can provide the desired value of confinement losses of the fundamental mode for the selected wavelength. We also demonstrate that an optimum configuration of the proposed design exists, for which the widest spectral range of the single-mode guidance of fibers can be obtained: from 0.2 to 2.3 microns.

3. Materials and Methods

Figure 1 shows cross section of the proposed BMSF. The distance between the adjacent holes in the first ring is Λ_1, except for two pairs of holes, which are more widely spaced ($\Lambda_{1W} > \Lambda_1$).

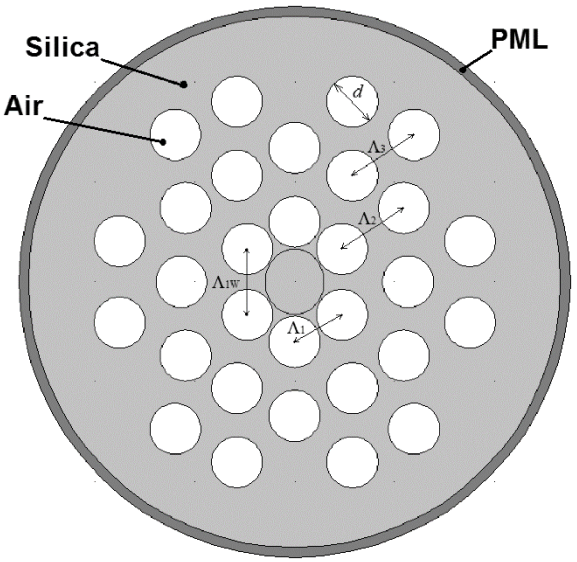

Figure 1. Cross section of the BMSF with e = 0.9; d/Λ_1 = 0.94; d/Λ_{1W} = 0.77; $d/\Lambda_2 = d/\Lambda_3$ = 0.69.

Each of the holes of the second ring is at a distance of $\Lambda_2 \geq \Lambda_1$ from the nearest hole(s) of the first ring. In addition, each of the holes of the third ring is at a distance of $\Lambda_3 \geq \Lambda_1$ from the nearest holes of the second ring. The third ring has only 12 holes so that the total number of holes is 30. The diameters of the core along the x- and y- axes are D_x and D_y, respectively. We define the BMSF core ellipticity as $e = D_x/D_y$.

The proposed design of the BMSF provides sufficient leakage losses for higher-order modes, which are critical in maintaining single-mode guidance (Wong et al., 2005; Dong et al., 2007). In addition, these BMSFs with a certain relationship between the width of wider bridges $Z_{1W} = (\Lambda_{1W} - d)$ and the core ellipticity e may have high birefringence and equal mode sizes along the two orthogonal axes (Denisov et al., 2015). Finally, additional possibilities

exist for optimization of the BMSF parameters when choosing various ratios of d/Λ_1, d/Λ_2 and d/Λ_3.

We calculated the confinement losses, birefringence and dispersion characteristics of the proposed BMSF using the finite element method (FEM) with a cylindrical perfectly matched layer (PML). This method can represent any arbitrary cross-section with different arrangement of air holes and has been widely used to find the modal solutions of a wide range of optical waveguides (Saitoh and Koshiba, 2002). We chose silica glass as the BMSF material and determined its refractive index using a Sellmeier equation (Agrawal, 1995). Calculations were performed for the BMSF core diameter D_y = 3.45 μm and the core ellipticity e = 0.9. For these parameters, we chose $\Lambda_{1W} = 1.22\times\Lambda_1$ to ensure equal mode sizes along the two orthogonal axes for FMs.

For each of the chosen ratio d/Λ_1, we determined the ratio d/Λ_2 (at the first stage, we selected $d/\Lambda_3 = d/\Lambda_2$), which provided confinement losses for the x-polarized FM 0.1 dB/m ±0.1% for the wavelength of 2.3 microns (Dong et al., 2007). In other words, we chose the long-wavelength boundary of single-mode guidance λ_{FM} to be 2.3 microns. For any specific practical purpose, the long-wavelength boundary λ_{FM} and the level of confinement losses for FMs for that wavelength should be defined individually.

We then calculated confinement losses for the x- and y-polarized FMs (designated as 1 and 2, respectively) and for four HOMs (designated from 3 to 6 in descending order of the real part of their effective refractive indexes) in the spectral range of 0.20 to 2.65 microns.

4. Results and Discussion

Figure 2 shows an example of intensity distributions of fundamental (1, 2) and higher (3–6) modes for the BMSF with ratio d/Λ_1 = 0.91 for the wavelength of 1.05 microns.

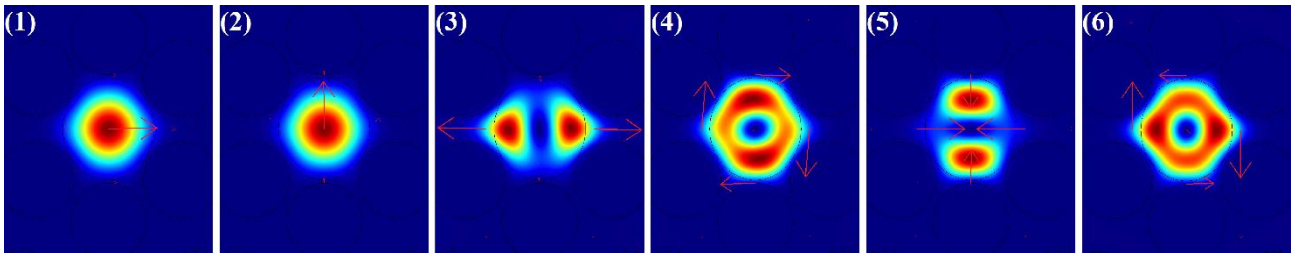

Figure 2. Intensity distributions of fundamental (1, 2) and higher (3–6) modes for the BMSF with ratio d/Λ_1 = 0.91 for the wavelength of 1.05 μm.

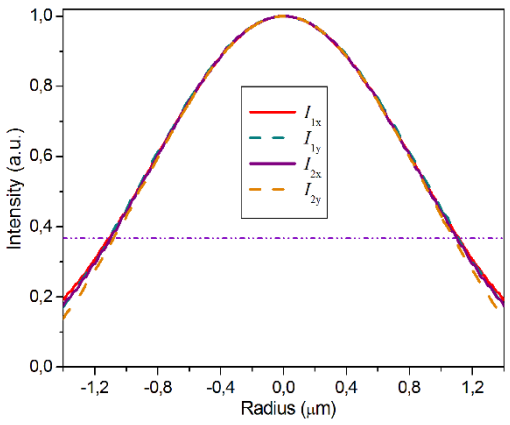

Figure 3. Radial dependences of the relative intensity distributions of fundamental modes (1, 2) in orthogonal directions (x, y) for the BMSF with d/Λ_1 = 0.94.

Figure 3 shows an example of calculated radial dependences of the relative intensity distributions I_{ab} of fundamental modes (a = 1, 2) in orthogonal directions (b = x, y) for the BMSF with d/Λ_1 = 0.94 for the wavelength of 1.55 microns. From the graph, we could determine mode field diameters (MFDs) of fundamental modes at the level 1/e of the maximum intensity: MFD_{1x} = 2.22 μm; MFD_{1y} = 2.22 μm; MFD_{2x} = 2.20 μm and MFD_{2y} = 2.16 μm.

Therefore, the mode field had equal sizes along the x- and y-axes for the x-polarized FM (Mode 1), but had slightly different sizes along the x- and y-axes for the y-polarized FM (Mode 2). However, for many practical applications, this difference in mode field sizes along the x- and y-axes (2%) has no significance.

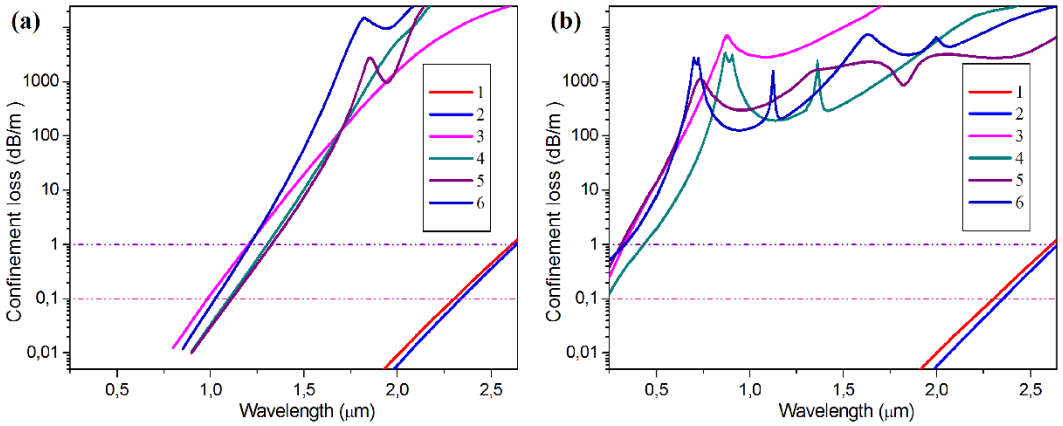

Figure 4. Spectral dependences of confinement losses of fundamental (1, 2) and higher (3–6) modes: a). For the BMSF with ratio $d/\Lambda_1 = 0.85$; b). For the BMSF with ratio $d/\Lambda_1 = 0.91$.

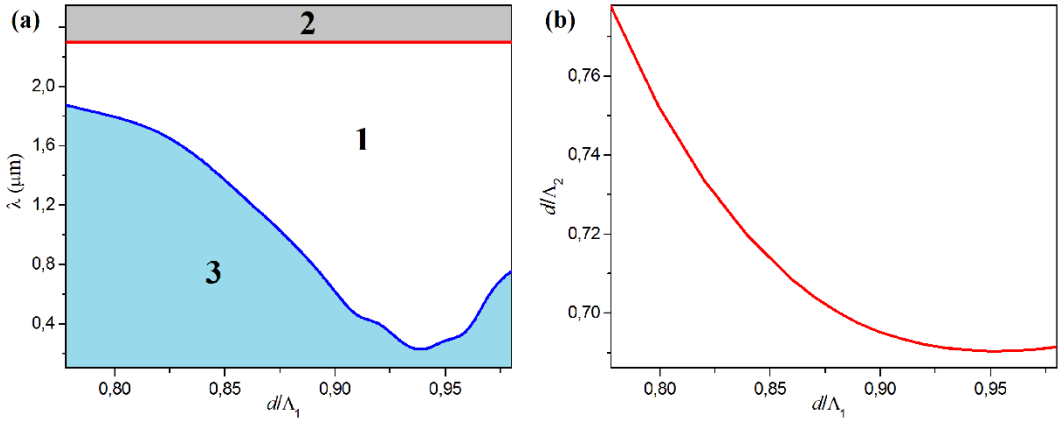

Figure 5. a). The dependence of the spectral range of the single-mode guidance (region 1) for the BMSF as a function of the ratio d/Λ_1; b). The dependence of the ratio d/Λ_2 as a function of the ratio d/Λ_1.

Figure 4,a shows an example of the spectral dependences of confinement losses of fundamental (1, 2) and higher (3–6) modes for the BMSF with ratio $d/\Lambda_1 = 0.85$ and Figure 4,b shows an example of the spectral dependences of confinement losses of FMs and HOMs for the BMSF with ratio $d/\Lambda_1 = 0.91$.

We defined the short-wavelength boundary of the single-mode guidance λ_{SM} as a wavelength for which confinement losses > 1.0 dB/m for all higher modes (Dong et al., 2007)

Figure 5,a shows the dependence of the spectral range of the single-mode guidance (region 1) for the proposed BMSF as a function of the ratio d/Λ_1. The red line in Figure 5,a indicates the value of λ_{FM} and the blue line indicates the value of λ_{SM}.

Therefore, region 2 presents an area where confinement losses for the *x*-polarized FM (Mode 1) > 0.1 dB/m and region 3 presents the area where confinement losses for any/all of HOMs < 1.0 dB/m.

Figure 5,b shows the dependence of the ratio d/Λ_2 as a function of the ratio d/Λ_1 which provided confinement losses for the *x*-polarized FM 0.1 dB/m ±0.1% for the wavelength of 2.3 microns.

From Figure 5,a we can see that for the chosen BMSF parameters (diameter of the core D_y, the core ellipticity *e* and the ratio Λ_{1W}/Λ_1) an optimum value of the ratio $d/\Lambda_1 = 0.94$ existed, for which the widest spectral range of the single-mode guidance was obtained: from 0.2 to 2.3 microns.

It is worth noting that the BMSF with the ratio $d/\Lambda_1 = 0.78$ corresponds to the case of $d/\Lambda_1 = d/\Lambda_2 = d/\Lambda_3$, and for this BMSF, the range of the single-mode guidance was significantly less, that is, from 1.9 to 2.3 microns.

As can be seen from Figure 4,a and Figure 4,b, spectral dependences of confinement losses of HOMs have complicated behavior with local maxima at different wavelengths. BMSFs with other ratios $d/\Lambda_1 \geq 0.82$ also have similar behavior of spectral dependences of confinement losses of HOMs with some other values of so called "resonance" wavelengths that depend on the ratio d/Λ_1.

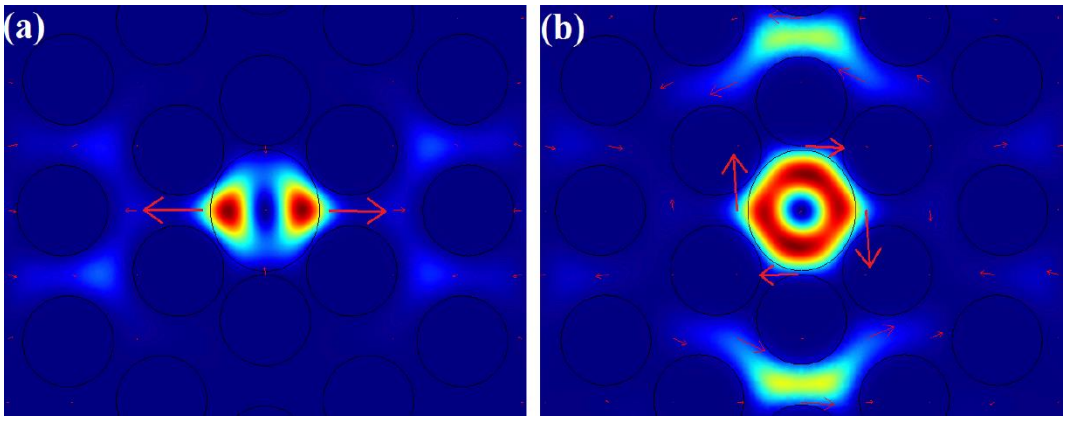

Figure 6. a). Intensity distribution of HOM 3 for the BMSF with ratio d/Λ_1 = 0.91 for the wavelength of 0.875 μm; b). Intensity distribution of HOM 4 for the BMSF with ratio d/Λ_1 = 0.91 for the wavelength of 1.363 μm.

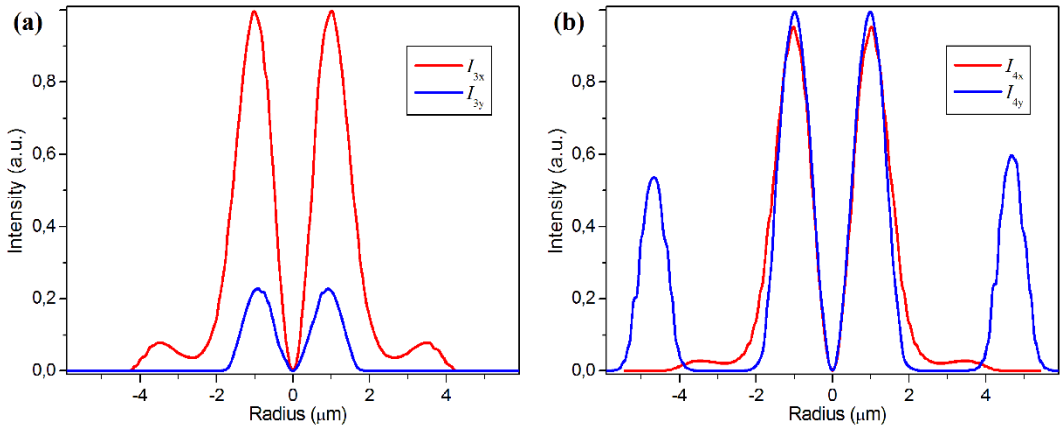

Figure 7. a). Radial dependences of the relative intensity distributions along the x- (I_{3x}) and y-axes (I_{3y}) of the HOM 3 for the wavelength of 0.875 μm; b). Radial dependences of the relative intensity distributions along the x- (I_{4x}) and y-axes (I_{4y}) of the HOM 4 for the wavelength of 1.363 μm.

To understand the underlying physical mechanism that is responsible for appearance of local maxima on spectral dependences of confinement losses of HOMs, Figure 6,a shows an example of spatial intensity distribution of HOM 3 for the BMSF with ratio d/Λ_1 = 0.91 for the wavelength of 0.875 μm (one of the resonance wavelength) and Figure 6,b shows an example of spatial intensity distribution of the HOM 4 for the wavelength of 1.363 μm (another resonance wavelength).

Figure 7,a shows radial dependences of the relative intensity distribution along the x- (I_{3x}) and y-axes (I_{3y}) of the HOM 3 for the wavelength of 0.875 μm. And Figure 7,b shows radial dependences of the relative intensity distribution along the x- (I_{4x}) and y-axes (I_{4y}) of the HOM 4 for the wavelength of 1.363 μm.

It is clear from Figure 6 and Figure 7 that HOM 3 and HOM 4 have some additional local maxima of intensity at resonance wavelengths. These local maxima of intensity are located in the cladding region of the BMSF and they are very close to the outer boundary of the cladding. Hence due to the presence of such additional local maxima of intensity these HOMs have additional leakage losses near their resonance wavelengths. HOM 5 and HOM 6 have also similar additional local maxima of intensity at their resonance wavelengths that are located in their specific area of the cladding region.

It is worth noting that there are some leaky cladding modes that have their maxima of intensity just in the region where HOMs have additional local maxima. But there is no clear physical mechanism that can explain mixing of HOMs with leaky cladding modes to enhance HOM's confinement losses, as proposed in (Fini, 2005).

The intermodal nonlinear effects have been considered in narrow band fiber amplifiers with LMA fibers, such as intermodal four-wave mixing (Bendahmane et al., 2018; Lesvigne et al., 2007). Authors (Lesvigne et al., 2007) have performed numerical and experimental study of supercontinuum generation. The broadband frequency generation was induced by an initial four-wave mixing process. Phase matching was ensured thanks to a microstructured multimodal fiber with a specific design. Authors (Bendahmane et al., 2018) have performed theoretical and experimental investigations of the process of seeded intermodal four-wave mixing in a graded-index multimode fiber. A detailed characterization of

the spectral and spatial properties of new generated spectral sidebands showed good agreement with theoretical predictions from the phase-matching conditions.

So, phase-matching conditions should be taken into account for some intermodal nonlinear effects, but, first, these nonlinear effects appear only for high intensity light levels, and second, both the second- and fourth-order dispersions must be included in the phase-matching conditions to get agreement between theoretical and experimental results (Bendahmane et al., 2018).

We assume that for MSFs with a small number of holes, as the BMSF proposed in the present study and MSFs proposed in (Fini, 2005; Tsuchida et al., 2007), it is more convenient and rigorous to consider the MSF's core and cladding as a whole. Then the physical mechanism of additional confinement losses of HOMs at resonance wavelengths may be simply and clear described as resonance influence of the MSF's geometry on the spatial intensity distribution of HOMs and, hence, on the appearance of additional local maxima of HOM's intensity close to the outer boundary of the cladding that lead to resonance enhancement of leakage losses.

As can be seen from Figure 4,b, all resonance local maxima of confinement losses of HOMs have sufficiently large values, of the order of 1000 dB/m, and at the same time these maxima have also high background level, about 100 dB/m, for the major part of the spectral range considered. Hence, we can conclude that spectral dependence of this background level has the predominant influence on the value of the short-wavelength boundary of the single-mode guidance λ_{SM}. The background level is determined by leakage losses and it depends on values of BMSF's bridges between different holes. For the first ring these bridges equal $Z_1 = (\Lambda_1 - d)$ and $Z_{1W} = (\Lambda_{1W} - d)$. For the second ring of holes these bridges depend on the ratio d/Λ_2 and also have different values (see Figure 1). And for the third ring these bridges depend on the ratio d/Λ_3 and have different values for different pairs of holes. We assume that such combination of different bridges between holes in different rings play the main role in achieving the wide spectral range of single-mode guidance for the proposed BMSF.

Group velocity dispersion (*GVD*) is one of the key parameters for supercontinuum generation. Figure 8 shows *GVD* of fundamental modes 1 and 2 as a function of the wavelength for the BMSF with $d/\Lambda_1 = 0.94$.

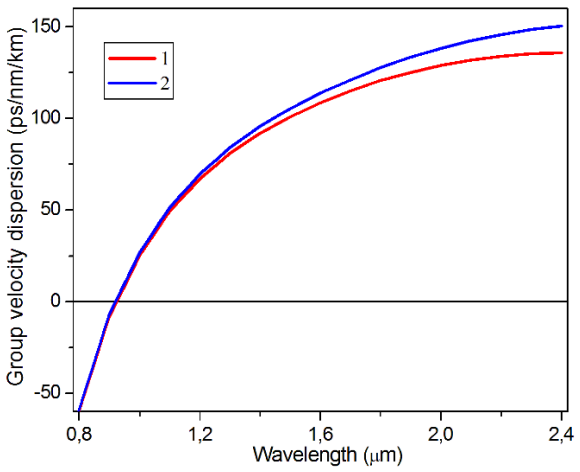

Figure 8. Group velocity dispersions of fundamental modes 1 and 2 as a function of the wavelength for the BMSF with $d/\Lambda_1 = 0.94$.

From the graph, we could determine zero dispersion wavelengths (*ZDW*s) for fundamental modes 1 and 2: $ZDW_1 = 926$ nm and $ZDW_2 = 924$ nm. These values of *ZDW*s were very close to the value of $ZDW = 925$ nm for the MSF with a hexagonal structure of holes and a circular core with a diameter $D = 3.27$ μm (i.e., with the same core area: $D^2 = e \times D_y^2$).

High value of birefringence is the key parameter for polarized supercontinuum generation. Figure 9 shows phase (B) and group (G) birefringence as a function of the wavelength for the BMSF with $d/\Lambda_1 = 0.94$. For example, for the wavelength of 1.55 microns, the group birefringence is $G = 6.4 \times 10^{-4}$.

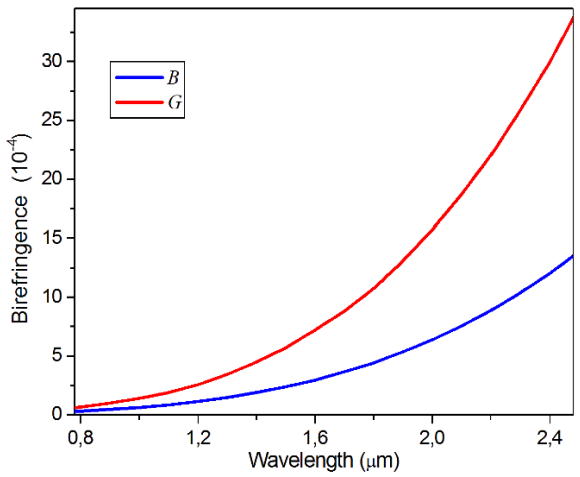

Figure 9. Phase (B) and group (G) birefringence as a function of the wavelength for the BMSF with $d/\Lambda_1 = 0.94$.

To fabricate the proposed BMSF, the technology of drilling holes in a monolithic silica preform may be used (Denisov et al., 2015). In contrast to the widespread stack-and-draw technique, this process allows any configuration of holes to be produced in the preform and, accordingly, in the fiber.

It is worth noting that for the ratio d/Λ_1 from 0.91 to 0.96, the short-wavelength boundary λ_{SM} of the

single-mode guidance of the proposed BMSF was less than 0.43 μm (see Figure 5,a). Therefore, this enables fabricating the fiber without tight parameter control.

To ensure the feasibility of the proposed BMSF's geometrical structure, it is important to examine in a detailed way the sensitivity of the BMSF's physical parameters, for example, the short-wavelength boundary of the single-mode guidance λ_{SM}, to technological deviations of the structure parameters of the fabricated BMSF from the ideal structure parameters.

First of all, we'll fabricate the proposed BMSF in the nearest future and will examine in a detailed way the geometrical parameters variations along some samples of fabricated BMSFs as we have performed earlier (Denisov et al., 2015). Then we'll introduce such variations of geometrical parameters in the proposed BMSF's structure and will perform numerical calculations of the BMSF's physical parameters. And finally, we'll compare results of numerical calculations of the simulated BMSF and experimental investigations of the fabricated one.

We assume that even small variations of geometrical parameters in the proposed BMSF's structure may have significant influence on the locations and magnitudes of resonance maxima of confinement losses. But it is unlikely that these variations may significantly change the background level of confinement losses. Hence, we suppose that small variations of geometrical parameters in the proposed BMSF's structure may lead to relatively small variations of the short-wavelength boundary of the single-mode guidance λ_{SM}.

These types of fibers may be used, for example, for polarized supercontinuum generation with high light-beam quality in a wide spectral range.

5. Conclusions

In conclusion, we have presented a new design of birefringent microstructured fibers with three rings of identical circular air holes around an elliptical core with different distances between the rings of holes. The first ring contains two pairs of holes, which are more widely spaced than others. We have calculated confinement losses for fundamental modes and higher-order modes for different BMSF's configuration parameters in the spectral range of 0.2–2.65 microns. We have discussed the underlying physical mechanism that is responsible for appearance of local maxima on spectral dependences of confinement losses of higher-order modes. The study showed that the proposed design makes it possible to obtain single-mode guidance of fibers in the spectral range of 0.2–2.3 microns.

Funding

The work was carried out within the framework of the state task.

References

Agrawal, G. P. (1995). Nonlinear Fiber Optics. New York: Academic Press.

Bendahmane, A., Krupa, K., Tonello, A., Modotto, D., Sylvestre, T., Couderc, V., Wabnitz, S., and Millot, G. (2018). Seeded intermodal four-wave mixing in a highly multimode fiber. *J. Opt. Soc. Am. B*, 35:295-301.

Birks, T. A., Knight, J. C., and Russell, P. St. J. (1997). Endlessly single-mode photonic crystal fiber. Opt. Lett., 22:961–3.

Denisov, A. N., Semjonov, S. L., Astapovich, M. S., and Senatorov, A. K. (2015). Highly Birefringent Microstructured Fibers With Low Mode Asymmetry. J. Lightwave Technol., 33:5184–94.

Dong, L., Peng, X., and Li, J. (2007). Leakage channel optical fibers with large effective area. J. Opt. Soc. Am. B, 24:1689–97.

Fini, J. M. (2005). Design of solid and microstructure fibers for suppression of higher-order modes. Opt. Express, 13:3477–90.

Klarskov, P., Isomäki, A., Hansen, K. P., Andersen, P. E. (2011). Supercontinuum generation for coherent anti-Stokes Raman scattering microscopy with photonic crystal fibers. Opt. Express, 19:26672–83.

Lesvigne, C., Couderc, V., Tonello, A., Leproux, P., Barthélémy, A., Lacroix, S., Druon, F., Blandin, P., Hanna, M., and Georges, P. (2007). Visible supercontinuum generation controlled by intermodal four-wave mixing in microstructured fiber. *Opt. Lett.*, 32:2173-5.

Mortensen, N. A., Folkenberg, J. R., Nielsen, M. D., and Hansen, K. P. (2003). Modal cutoff and the V parameter in photonic crystal fibers. Opt. Lett., 28:1879–81.

Nielsen, F. D., Pedersen, M. Ø., Qian, Y., Andersen, T. V., Leick, L., Hansen, K. P., Pedersen, C. F., Thomsen, C. L. (2007). High power polarization maintaining supercontinuum source. CLEO/Europe and IQEC 2007 Conference Digest, (Optical Society of America), paper CJ5_4.

Saini, T. S., Kumar, A., and Sinha, R. K. (2016). Asymmetric large-mode-area photonic crystal fiber structure with effective single-mode operation: design and analysis. Appl. Opt., 55:2306–11.

Saitoh, K., and Koshiba, M. (2002). Full-vectorial Imaginary-Distance Beam Propagation Method Based on a Finite Element Scheme: Application to Photonic Crystal Fibres. IEEE J. Quantum Electron., 38:927-33.

Saitoh, K., Varshney, S., Sasaki, K., Rosa, L., Pal, M., Paul, M. C., Ghosh, D., Bhadra, S. K., and Koshiba, M. (2011). Limitation on Effective Area of Bent Large-Mode-Area Leakage Channel Fibers. J.

Lightwave Technol., 29:2609-15.

Tsuchida, Y., Saitoh, K., and Koshiba, M. (2007). Design of single-moded holey fibers with large-mode-area and low bending losses: The significance of the ring-core region. Opt. Express, 15:1794–803.

Wong, W. S., Peng, X., McLaughlin, J. M., and Dong, L. (2005). Breaking the limit of maximum effective area for robust single-mode propagation in optical fibers. Opt. Lett., 30:2855–7.

Xiong, C., and Wadsworth, W. J. (2008). Polarized supercontinuum in birefringent photonic crystal fibre pumped at 1064 nm and application to tuneable visible/UV generation. Opt. Express, 16:2438–45.